Biointerface Research in Applied Chemistry
Open-Access Journal (ISSN: 2069-5837)

Article
Volume 13, Issue 3, 2023, 233
https://doi.org/10.33263/BRIAC133.233

In silico Investigations on Structure, Reactivity Indices, NLO properties, and Bio-evaluation of 1-benzyl-2-phenyl-1*H*-benzimidazole Derivatives using DFT and Molecular Docking Approaches

Asiata Omotayo Ibrahim [1], Banjo Semire [1,*], Adewusi John Adepoju [1], Dayo Felix Latona [2], Abel Kolawole Oyebamiji [3], Abayomi Dele Owonikoko [4], Tofunmi Emmanuel Oladuji [1], Olusegun Ayobami Odunola [1,5,*]

1 Computational Chemistry Laboratory, Department of Pure and Applied Chemistry, Ladoke Akintola University of Technology, P.M.B. 4000, Ogbomoso, Oyo-State, Nigeria; bsemire@lautech.edu.ng (B.S.);
2 Department of Pure and Applied Chemistry, Osun State University, Osogbo, Nigeria; Dayo.latona@uniosun.edu.ng (D.F.L.);
3 Department of Basic Sciences, Adeleke University, P.M.B. 250, Ede, Osun State, Nigeria; abeloyebamiji@gmail.com (A.K.O.);
4 Department of Chemistry, Emmanuel Alayande College of Education, Oyo State, Nigeria
5 Department of Chemistry, Faculty of Natural and Applied sciences, Hallmark University, Ijebu-Itele, Ogun state, Nigeria; oaodunola@lautech.edu.ng (O.A.O.);
* Correspondence: bsemire@lauctech.edu.ng (B.S.); oaodunola@lautech.edu.ng (O.A.O.);

Scopus Author ID 57189714998
Received: 7.01.2022; Accepted: 5.02.2022; Published: 6.06.2022

Abstract: Six 1-benzyl-2-phenyl-1*H*-benzimidazole derivatives, A1-A6, were modeled computationally, and equilibrium optimization was carried out at the B3LYP/6-31G** level of theory. The geometrical parameters, IR, UV-Vis, and molecular reactive properties were predicted on the basis of density functional theory (DFT) calculations. The electron-donating/accepting power ($\omega-/\omega+$) calculated were 4.71/1.18, 5.675/1.766, and 4.785/1.210 eV for **A1, A2,** and **A3**, respectively, indicating good electron donors; while **A4** and **A5** were calculated to be 8.13/3.60 and 9.284/4.744 eV, respectively signifying good electron acceptors in line with chemical hardness (μ), electrophilicity (ω) values and MEP analysis. The NLO behavior of compounds **A1-A3** was greater than that of the standard NLO material urea gives the most reactive sites in the molecules. Docking analysis revealed that binding affinities for the six compounds A1-A6 were -8.3 to -9.0 kcal/mol and -9.2 to -10.0 kcal/mol for APO-liver alcohol dehydrogenase inhibitor (PDB IP: 5ADH) and antihypertensive protein hydrolase inhibitor (PDB IP: 4XX3), respectively; thus could possess good antioxidant and antihypertensive properties.

Keywords: 1-benzyl-2-phenyl-1*H*-benzimidazole; molecular descriptor; NLO; molecular docking.

1. Introduction

Imidazole is a five-member nitrogen-containing heterocyclic compound that plays a vital role in synthetic chemistry as a mediator for synthetic reactions [1]. The incorporation of electron-rich imidazole moieties has become essential in designing, developing, and improving imidazole-based drugs in pharmaceutical industries [2,3]. Imidazole derivatives are fundamental and vital component of some pharmaceutical drugs such as clotrimazole, olmesartan, biotin, ketoconazole, losartan and eprosartan [4-6]. They are used as green solvents

in ionic liquids [7] and have outstanding biological activities as antitumor, antiplasmodial, antibacterial, anti-inflammatory, and antifungal [8-12]. The human body is made up of essential components that are imidazole nucleus based; these include Vitamin B12, histidine, purines, and biotin [13, 14].

In addition, Benzimidazole derivatives consist of a fused benzene ring with an imidazole nucleus is another set of imidazoles that has also been of great interest in biological, medical, and clinical research due to their associated various pharmacokinetic properties [15, 16] and promising pharmacological activities notably their wide-ranging therapeutic actions such as antimicrobial, anticancer, antidiabetic, antihistamine, analgesics, antiparasitic and antiviral [17-25]. This class of heterocyclic aromatic compounds has been reported to treat cardiovascular, neurology, ophthalmology, and endocrinology disorders [25-27]. They are useful in controlling the diseases such as Ischemia-reperfusion injury, hypertension, and obesity. In addition, they serve as a good inhibitor of a number of enzymes. They are extensively being used in the synthesis of organic intermediates. Therefore, great attention has been placed on synthesizing benzimidazole derivatives for their biological and pharmaceutical explorations.

The ability of the imidazole ring and its related compounds, such as benzimidazole, to easily accommodate functional groups, thereby enabling the interaction covalently with the NLO chromophores in polyamides, has led to the development of NLO polymers [28, 29]. The adaptability of imidazole derivatives is a great property for their exploration as optoelectronic and supra-molecular materials [30, 31]. In doing this, functional groups are always being used to turn or modulate the structural, electronic, and frontier orbitals properties of the imidazoles in order to understand NLO properties such as first-order nonlinear properties, second-order nonlinear optical properties, hyperpolarizability, and thermal stability which are imperial to design functional NLO materials [30-35].

In recent years, density functional theory has become a veritable method in providing an admirable interpretation of experimental data and qualitative prediction of molecular properties and reactivity descriptions of chemical systems [36-39].DFT is often used to explain the drug molecule's reaction mechanisms and precisely calculate the transition state of a reaction mechanism, which is vital for drug design. [40]. Moreover, theoretical calculations have become a prominent tool in designing functional materials with good charge transport properties and high-efficient charge transport [41-48]. Recently, Manikandan *et al.*, investigated two imidazole derivatives; 1-(2,4-difluorobenzyl)-2-(2,4-difluorophenyl)-6-methyl-*1H*benzo[d]imidazole and 1-(4-(trifluoromethyl)benzyl)-2-(4-(trifluoromethyl)phenyl)-6-methyl-*1H*-benzo[d]imidazole using experimental and theoretical methods. The frontier orbitals, polarizability, hyperpolarizability, and NLO properties of the two compounds were examined via DFT method at DFT/B3LYP/6-31G(d,p) level of theory [49]. The results revealed that the imidazole derivatives are promising applications in various nonlinear optical (NLO) devices due to their significant values of molecular hyperpolarizabilities and fine microscopic NLO behavior. Also, the results showed that the high NLO responses of the donor-acceptor π-conjugated compounds are related to the intramolecular charge transfer excited state [48, 49].

Therefore, in furtherance of exploration of inherent properties of 1-(2,4-difluorobenzyl)-2-(2,4-difluorophenyl)-6-methyl-1Hbenzo[d]imidazole as examined by Manikandan *et al*. [49], DFT calculations were on 2-[3,4-difluorophenyl]-3-[3,4-difluorophenyl]methyl]-5-methyl-*3H*-Imidazole (**A1)**, 2-[3-fluoro-4-[trifluoromethyl]phenyl]-

3-[3-fluoro-4-[trifluoromethyl]phenyl]methyl]-5-methyl-*3H*-imidazole (**A2**), 5-methyl-2-[2,3,4-trifluorophenyl]-3-[2,3,4-trifluorophenyl]methyl]-*3H*-imidazole (**A3**), 5-methyl-2-[4-nitro-phenyl]-3-[4-nitrophenyl]methyl]-*3H*-imidazolee **(A4),** 5-methyl-2-[2-nitro-4-(trifluoromethyl]phenyl-3-[2-nitro-4-[trifluoromethyl]phenyl]methyl]-*3H*-imidazole **(A5)** and [2-fluoro-6-[2,-[3-fluoro-2-amino-4-[trifluoromethyl]phenyl-5-methyl-*3H*-indo-3 yl]methyl]-3-[trifluoromethyl]phenyl]-*1H*-imidazole (**A6**) by modifying 1-(2,4-difluorobenzyl)-2-(2,4-difluorophenyl)-6-methyl-*1H*benzo[d]imidazole with functional groups as shown in Figure 1. The properties examined were frontier molecular orbitals, dipole moment, (μ), reactivity indices, polarizability (α), hyperpolarizability (β), nonlinear optical properties and charge distributions, and also molecular docking simulation to examine the bio-usefulness of these compounds as antioxidant and antihypertensive agents.

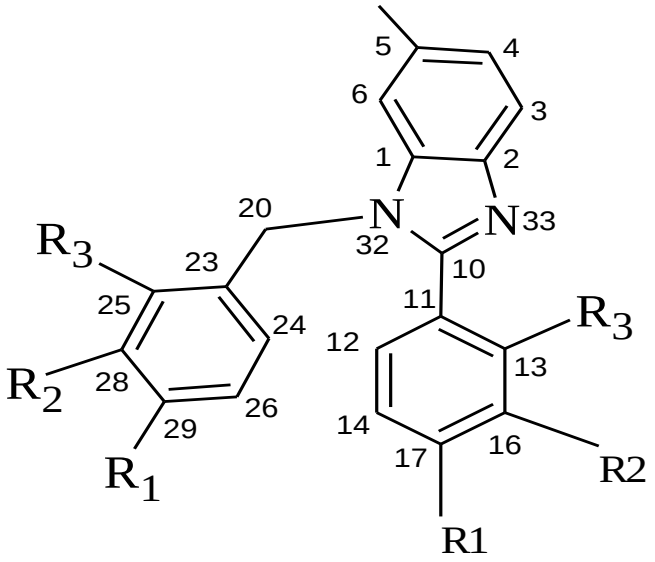

	R1	R2	R3	Molecular Formula
A1	F	F	H	$C_{21}H_{14}F_4N_2$
A2	CF_3	F	H	$C_{23}H_{14}F_8N_2$
A3	F	F	F	$C_{21}H_{12}F_6N_2$
A4	NO_2	H	H	$C_{21}H_{16}N_4O_4$
A5	CF_3	H	NO_2	$C_{23}H_{14}F_6N_4O_4$
A6	CF_3	NH_2	H	$C_{23}H_{18}F_6N_4$

Figure 1. Schematic structure and numbering of studied compounds.

2. Materials and Methods

The equilibrium conformer searching was carried out on the imidazole derivatives using the semi-empirical AM1 method to find the lowest conformer for each compound. This was then taken as starting structure for DFT calculations [50]. The optimization of these compounds was performed with DFT of Becke's three-parameter hybrid functional with a correlation of Lee, Yang, and Parr (B3LYP) [51] with a 6-31G** basis set. Frequency calculations were examined to ascertain minima equilibrium characterized by positive harmonic frequencies [52, 53] as implemented in Spartan 14 [54]. The DFT hybrid B3LYP functional has been described to overestimate the fundamental modes; thus scaling factor of 0.9619 has been recommended for frequency calculated at B3LYP/6-31G** was used to give frequencies considerably in agreement with experimental data [55]. Still, in this work, the unscaled vibrational modes were compared with experiment [49]. The molecular properties calculated from conceptual DFT were electron affinity (EA = $-E_{LUMO}$), ionization potential (IP = $-E_{HOMO}$), chemical potential

(μ), chemical hardness (η), global nucleophilicity/electrophilicity (ω), electron-accepting power ($\omega+$) and electron-donating power (ω^-) [56-59] as shown in equations 1 to 5:

$$\mu = \frac{-E_{LUMO} + E_{HOMO}}{2} \approx \frac{IP + EA}{2} \quad (1)$$

$$\eta = \frac{E_{LUMO} - E_{HOMO}}{2} \approx \frac{IP - EA}{2} \quad (2)$$

$$\omega = \frac{\mu^2}{2\eta} = \frac{(IP+EA)^2}{4(IP-EA)} \quad (3)$$

$$\omega^+ = \frac{(IP+3EA)^2}{16(IP-EA)} \quad (4)$$

$$\omega^- = \frac{(3I+A)^2}{16(I-A)} \quad (5)$$

3. Results and Discussion

3.1. Geometries.

The molecular geometries of **A1-A6** optimized at DFT/6-31G** method are displayed in Figure 2 and Table 1; they were compared with 1-(2,4-difluorobenzyl)-2-(2,4-difluorophenyl)-6-methyl-1Hbenzo[d]imidazole (**Aa**) as reported by Manikandan *el at.*, [49]. The C_1-N_{32} bond has a single bond character with the bond length of 1.1.389Å for **A6**, whereas it was reported as 1.405Å for **Aa** [49]; thus, the C_1-N_{32} bond length in **A6** was shortened by 0.016 Å. This bond was reported as 1.4163 and 1.4159 Å for 2-chloro-4,5-dimethyl-1-phenyl-1H-imidazole and 2-chloro-4,5-dimethyl-1-(o-tolyl)-1H-imidazole respectively [60]. However, C_1 –N_{32} bond length was calculated to be 1.391 Å for **A1**, 1.391 Å for **A2**, 1.389 Å for **A3**, 1.392 Å for **A4,** and 1.391 Å for **A5,** respectively. This showed that the C_1-N_{32} bond length for the model compounds was shortened by ≈ 0.07 Å an, indicating double-bond character and reflected the effect of resonance on the compounds compared to **Aa** [6, 61]**.** Therefore, the shortening of the terminal C_1-N_{32} bond in the sigma center for **A1-A6** compared to the **Aa** analog should lead to a higher vibrational frequency of terminal C=C bonds for model compounds [62-64]. Also, the C_{10}-N_{33} bond in the imidazole ring act as a double bond character with the bond length of 1.396 Å for **A1**, 1.396 Å for **A2**, 1.393 Å for **A3**, 1.397 Å for **A4**,1.393 Å for **A5** and 1.316 Å for **A6** respectively. However, C_{10}-N_{33} were calculated to be 1.4809Å for **Aa** [49], 1.307 and 1.3074 Å in 2-chloro-4,5-dimethyl-1-phenyl-1H-imidazole and 2-chloro-4,5-dimethyl-1-(o-tolyl)-1H-imidazole, respectively [60], this showed that C_{10}-N_{33} was shortened by 0.0849 Å for **A1**, 0.0849 Å for **A2**, 0.0879 Å for **A3**, 0.839 Å for **A4**, 0.0879 Å for **A5**, 0.1649 Å for **A6** respectively (Table 1). The C_{10}-N_{33} bond of model compounds slightly exhibited a double bond character which was pronounced in **A6** due to the presence of NH_2 that helped in the delocalization of electrons via its lone pair of electrons. The C_1-C_2 bond length in the imidazole ring was calculated to be 1.412 Å for **A1**, 1.411 Å for **A2**, 1.412 Å for **A3**, 1.412 Å for **A4**, 1.409 Å for **A5,** and 1.412 Å for **A6,** respectively, but calculated to be 1.3208 Å for **Aa.** This showed that the C_1-C_2 bond length in model compounds was elongated

compared to **Aa,** thereby displaying a normal single bond character. The C_{10} –C_{11} bond lengths were calculated to be 1.474 Å for **A1**, 1.474 Å for **A2**, 1.474 Å for **A3**, 1.472 Å for **A4**, 1.489 Å for **A5,** and 1.475 Å for **A6** respectively, but calculated to be 1.5400 Å for **Aa**.

The bond angles of C_1 –N_{32}-C_{10} are 105.84º, 105.79º, 105.92º, 105.79º, 105.59 º, and 124.25 º for **A1** to **A6,** respectively. However, N_{32}-C_{10}-N_{33} are 113.05 º for **A1**, 113.07 º for **A2**, 113.05 º for **A3**, 112.93 º for **A4**, 113.38 º for **A5,** and 113.04 º for **A6**. The little differences observed in bond angles in the imidazole derivatives are brought about by planarity differences as reflected in their dihedral angles (Table 1). It is caused by the substituted phenyl-imidazole ring at the para, meta, and ortho positions, as presented in Figures 1 and 2.

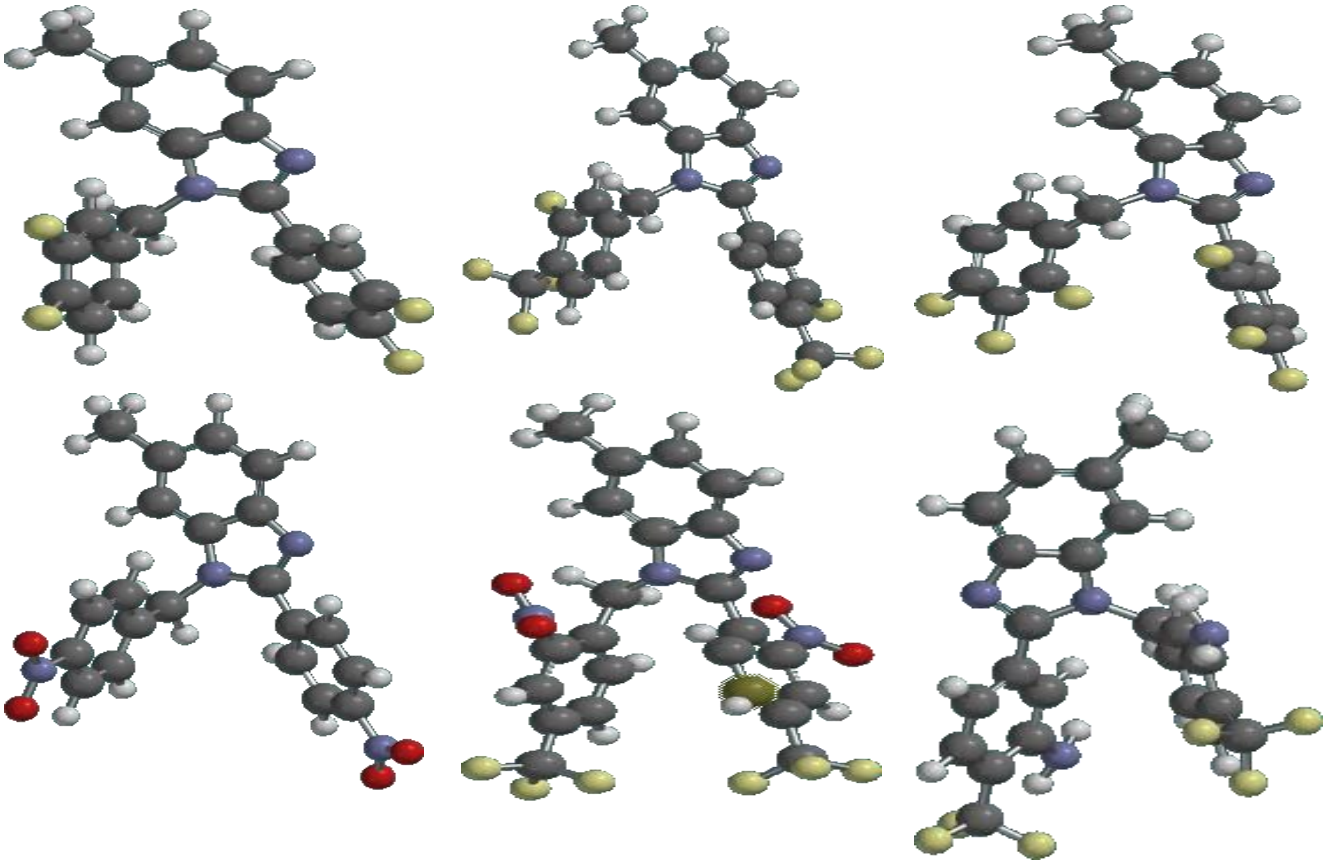

Figure 2. The optimized structures of model compounds.

Table 1. The Selected geometries of the studied imidazole derivatives.

	A1	**A2**	**A3**	**A4**	**A5**	**A6**	**Aa***
Bond Distance (Å)							
C1-C2	1.412	1.411	1.412	1.412	1.409	1.412	1.3208
C1-N32	1.391	1.391	1.389	1.392	1.391	1.379	1.4605
N32-C10	1.396	1.396	1.393	1.397	1.393	1.395	1.4809
C10-N33	1.315	1.315	1.316	1.316	1.311	1.316	1.3105
C10-C11	1.474	1.474	1.474	1.472	1.489	1.466	1.5400
C20-N32	1.465	1.464	1.464	1.460	1.460	1.455	1.4700
C20-C23	1.519	1.520	1.518	1.521	1.517	1.520	1.5400
C5-C38	1.511	1.511	1.511	1.511	1.511	1.511	1.5400
Bond Angle (˚)							
C1-N32-C10	105.84	105.79	105.92	105.79	105.59	100.00	100.94
C1-N32-C20	123.99	124.17	124.56	123.99	123.49	124.25	113.66
N32-C10-N33	113.05	113.07	113.05	112.93	113.38	113.04	111.59
C1O-C11-C12	122.70	122.69	123.71	122.79	116.18	121.71	120.00
N32-C20-C23	114.54	114.11	113.42	91.10	115.19	114.27	109.47
C20-C23-C24	121.30	120.69	122.23	121.30	124.75	119.71	120.00
C20-C23-C25	119.44	120.11	120.14	119.44	118.70	120.68	120.00

	A1	A2	A3	A4	A5	A6	Aa*
C4-C5-C38	119.77	119.61	119.64	119.56	119.60	119.73	119.86
Dihedral Angle (°)							
C1-N32-C10-N33	-0.75	0.76	0.44	-0.78	2.77	0.58	17.02
C1-C6-C5-C38	178.99	-179.88	-179.05	179.77	-179.86	-178.47	-179.78
C1-N32-C20-C23	-93.05	90.62	-96.70	-92.57	-122.05	92.21	-62.52
N32-C10-C11-C12	44.23	-43.15	-48.00	-142.05	-122.21	-45.82	-0.25
C23-C24-C26-C29	-0.37	0.20	0.14	-0.15	-2.49	0.54	-0.01
C1-C2-N33-C10	0.25	-0.42	-0.29	0.43	1.75	-0.41	4.04
C5-C6-C1-N32	-179.57	179.23	179.54	-179.83	179.46	179.46	176.00
C6-C1-C2-N33	179.16	-179.30	-179.49	178.75	179.62	-179.08	-172.97

Aa*; 1-(2,4-difluorobenzyl)-2-(2,4-difluorophenyl)-6-methyl-1Hbenzo[d]imidazole taken from [49].

3.2. Frontier molecular orbital analysis.

The frontier molecular orbitals, i.e., the highest occupied molecular orbital (HOMO), lowest unoccupied molecular orbital (LUMO), and HOMO-LUMO band gaps, as shown in Figure 3, are very important parameters for the understanding of chemical reactivity, kinetics stability, and photochemical properties [65-69]. The frontier orbital energies (E_{HOMO}, E_{LUMO}, and ΔE_g) are -5.88, 1-18, and 4.70 eV for **A1**; -6.13, -1.69, and 4.44 eV for **A2**; -5.94, -1.21 and 4.73 eV for **A3**; -6.27, -2.71 and 3.56 eV for **A4**; -6.05, -3.03 and 3.02 eV for **A5**, and -6.81, -1.25 and 5.56 eV for **A6** (Table 2 and Figure 3), this showed that NO_2 substituent profound effect in lowing the bandgap energy as reflected in **A4** and **A5** than Fluorine [70]; thus **A4** and **A5** should be the good acceptor of electrons from electron-rich molecules in line with electron affinity values (Table 2). The calculated chemical descriptors such as chemical potential (μ), chemical hardness (η) and global electrophilicity (ω) are -3.53, 2.35 and 2.651 eV for **A1**; -3.91, 2.22 and 3.443 eV for **A2**; -3.575, 2.365, and 2.702 eV for **A3**; -4.49, -1.78 and 5.663 eV for **A4**; -4.54, 1.58 and 6.825 eV for **A5**; -4.03, 2.78 and 2.921 eV for **A6**. The μ and ω values for **A4** and **A5** compounds collaborated that they are good electron acceptors. The electron-donating power (ω^-) and electron-accepting power (ω^+) have been attributed to the ability of a molecule to release electrons and to accept electrons, respectively; a smaller value of ω^- corresponds to a better donor of electron density and a greater ω^+ value corresponds to a better accepting electron capacity. The values for ω^- showed that **A1, A2,** and **A3** are good electron donors, while ω^+ revealed the tendency of **A4** and **A5** to be good electron acceptors in line with μ and ω values (Table 2).

Table 2. Frontier Molecular Orbital Analysis M1-M6.

Parameter	A1	A2	A3	A4	A5	A6
HOMO	-5.88	-6.13	-5.94	-6.27	-6.05	-6.81
HOMO -1	-6.22	-6.41	-6.22	-6.61	-6.21	-5.82
HOMO-2	-6.91	-7.30	-7.12	-7.71	-7.62	-5.91
LUMO	-1.18	-1.69	-1.21	-2.71	-3.03	-1.25
LUMO+1	-0.71	-1.32	-0.80	-2.61	-3.03	-0.82
ΔE_g	4.70	4.44	4.73	3.56	3.02	5.56
I	5.88	6.13	5.94	6.27	6.05	6.81
A	1.18	1.69	1.21	2.71	3.03	1.25
χ	3.53	3.91	3.575	4.49	4.54	4.03
μ	-3.53	-3.91	-3.575	-4.49	-4.54	-4.03
ŋ	2.35	2.22	2.365	1.78	1.51	2.78
ω	2.651	3.443	2.702	5.663	6.825	2.921
ω+	1.18	1.766	1.21	3.64	4.744	1.254
ω^-	4.71	5.676	4.785	8.13	9.284	5.284
$\sigma = 1/2\eta$	0.213	0.225	0.211	0.281	0.331	0.180

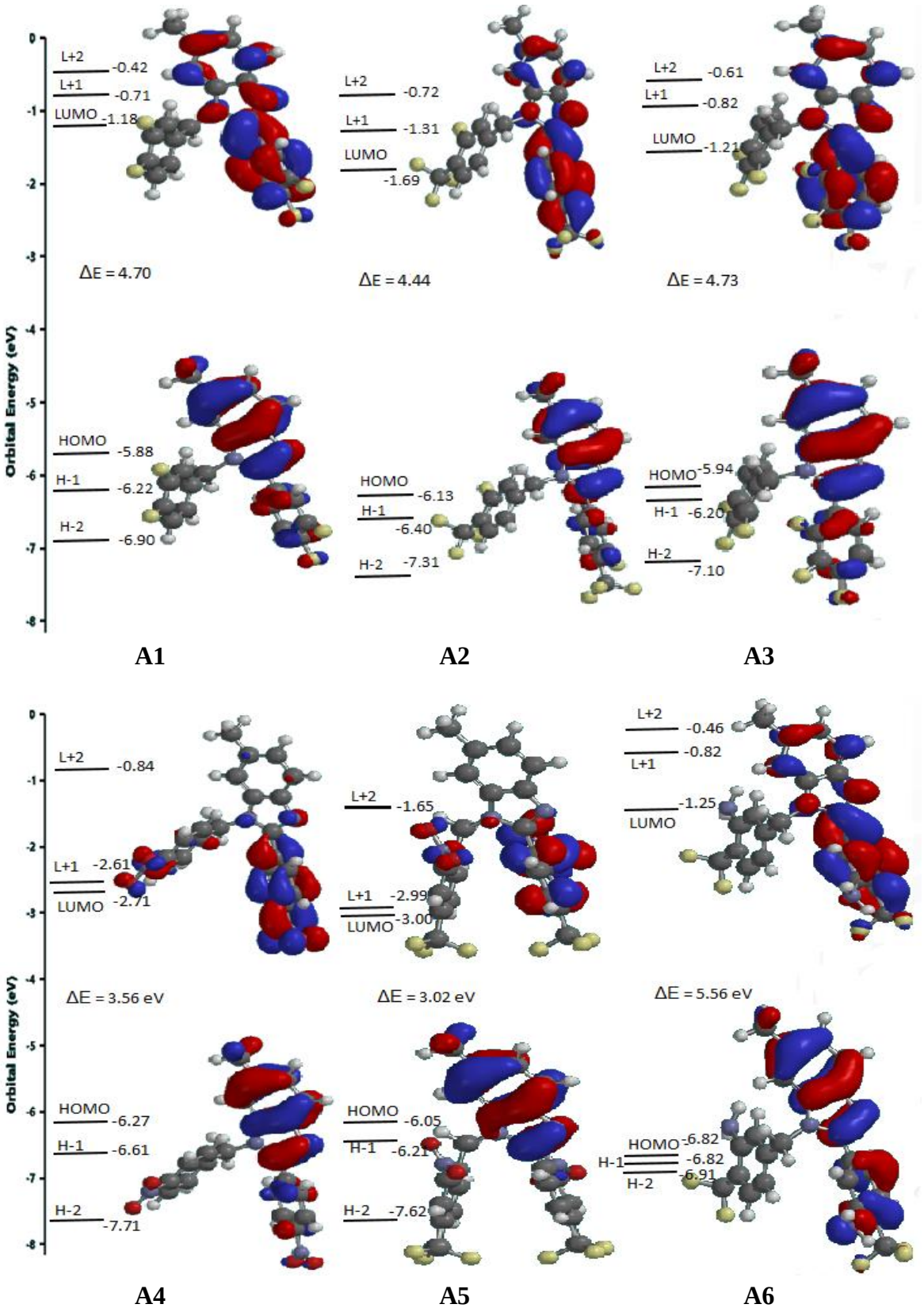

Figure 3. The highest occupied molecular orbital (HOMO) and the lowest unoccupied for **A1-A6**.

Furthermore, the electrostatic potential V(r) shows the static distribution of charges in three dimensions on a molecule related to molecular shapes, sizes, charge densities, and electrostatic potential reactive sites in the molecules [71]. This is a useful parameter for predicting and analyzing the initial site of attack for an approaching electrophile or nucleophile [72]. The MEP of the model compounds was simulated and analyzed from the optimized structures in their ground state, as displayed in Figure 4. The blue region corresponds to the

positive electrostatic potential, or electron-deficient region is localized mainly on the hydrogen atoms, whereas the red or yellow color, which represents a negative electrostatic potential or electron-rich area, is mainly situated on the acceptor moiety; the green color signifies essentially zero potential region [72, 73]. Therefore, electrostatic potential colour is usually ranged as red < orange < yellow < green < blue [72]. The negative (red) region is on one of the nitrogen atoms of the imidazole ring, which shows a possible site of attack for an electrophile.

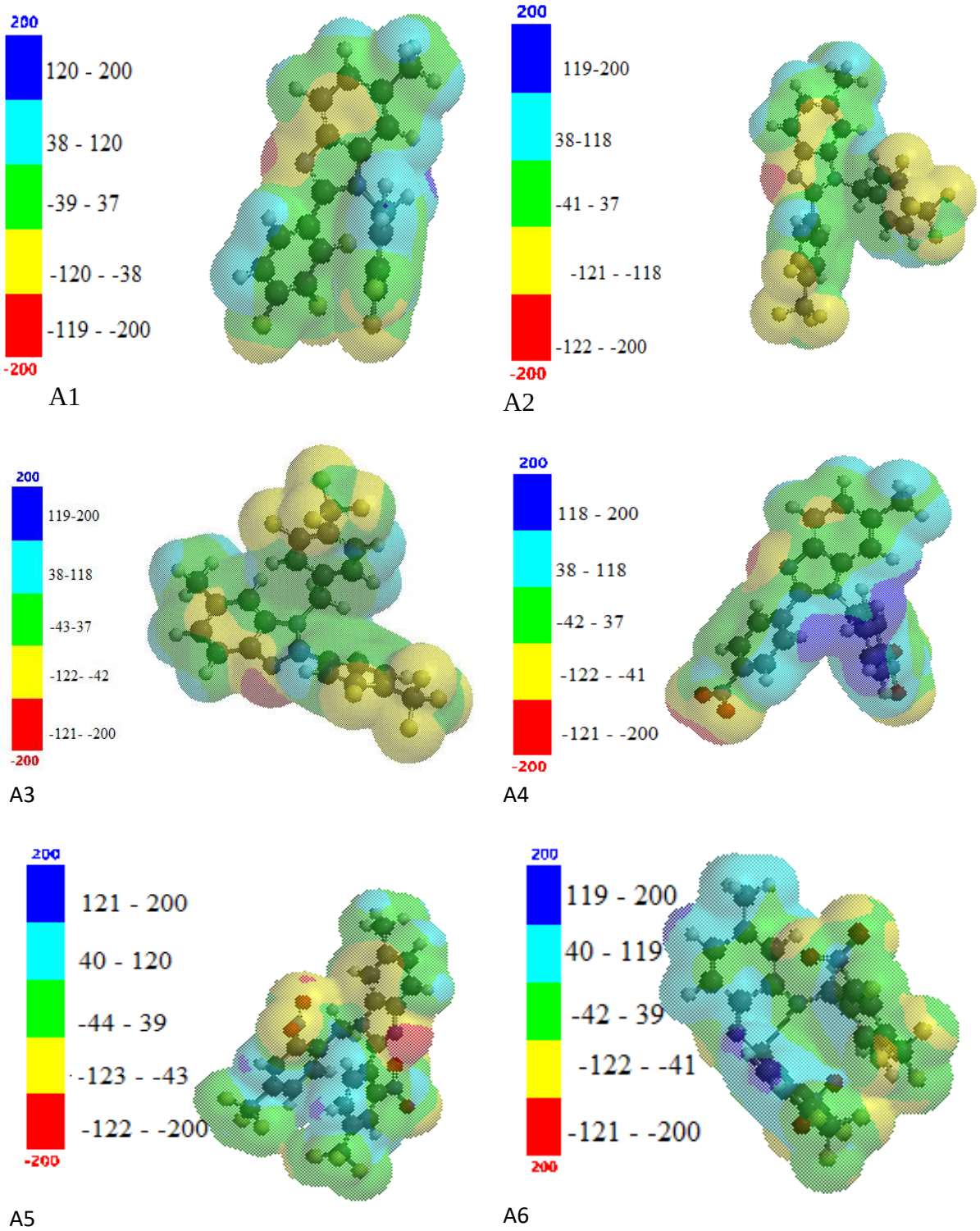

Figure 4. Molecular electrostatic potential (MEP) diagram of molecule **A1-A6**.

The **A3** and **A4** have an additional negative (red) region on the nitro group due to excess electrons as a result of pulling or drawing ability which may affect $\pi - \pi$ stacking arrangement

of these molecules. MEP analysis revealed that the imidazole ring's nitrogen atom is a center of electrophilic attacks.

3.3. Vibration Frequencies (cm^{-1}).

Vibrational frequency has been a powerful tool widely used in organic chemistry to identify functional groups of organic compounds and distinguish molecular conformers, tautomers, and isomers [74]. Properly comparing the theoretical data with experimental vibrational modes is always helpful in proper assignment and understanding of a fairly intricate system. Vibrational modes of compounds **A1–A6** were calculated at DFT- B3LYP/6-31G (d,p) level of theory were and compared with 1-(2,4-difluorobenzyl)-2-(2,4-difluorophenyl)-6-methyl-1Hbenzo[d]imidazole [49], and some important vibration modes computed were listed in Table 3. The IR frequency values in Table 3 showed that the DFT method used overestimated the vibrational frequencies, but the values are still in good agreement with the experimental data. A methyl group (which is generally referred to as an electron giving group) present in the observed molecule produced one asymmetric and one symmetric stretching vibration. The $–CH_2-$ asymmetric stretching vibrations observed were 3136 cm^{-1} for **A1**, 3155 cm^{-1} for **A2**, 3187 cm^{-1} for **A3**, 3132 cm^{-1} for **A4,** 3142 cm^{-1} for **A5** and 3176 $1cm^{-1}$ for **A6** respectively. Likewise, the $–CH_2-$ symmetric vibrations were calculated at 3084 cm^{-1} for **A1**; 3086 cm^{-1} for **A2**; 3097 cm^{-1} for **A3**; 3077 cm^{-1} for **A4**; 30385 cm^{-1} for **A5** and 3082 cm^{-1} for **A6** respectively. These were calculated to be 3170 and $3068cm^{-1}$ symmetric and asymmetric stretching vibrations, respectively [75], but it was experimentally observed at 2935 cm^{-1} [49]. The aromatic C-H asymmetric vibrations for A1-A6 are 3236, 3223, 3215, 3208, 3196 and 3181 cm^{-1} for **A1**; 3240, 3232, 3220, 3210 and 3182 $cm^{-1}$for **A2**; 3238, 3184 and 3179 cm^{-1} for **A3**; 3249, 3228, 3212 and 3190 cm^{-1} for **A4**; 3255, 3246, 3220 and 3214 $cm^{-1}$for **A5**; 3236, 3245, 3224 and 3214 cm^{-1} for **A6**. The C-H symmetric vibrations for are 3225, 3212 and 3184 cm^{-1} for **A1**; 3229, 3214, 3184 cm^{-1} for **A2**; 3232 and 3224 cm^{-1} for **A3**; 3247 and 3215 cm^{-1} for **A4**; 3232, 3227, 3213 and 3203 cm^{-1} for **A5**; 3236, 3230 and 3209 for **A6**, but calculated to be in region of $3198cm^{-1}$ and scaled to 3071 [70]. The C-H in-plane bending vibrations were 1233-1143 cm^{-1} for **A1**; 1326-1138 cm^{-1} for **A2**; 1322-1160 cm^{-1} for **A3**; 1324-1164 cm^{-1} for **A4**; 1318-$1235cm^{-1}$ for **A5**, and 1330-1154 cm^{-1} for **A6**. The C-H out of plane vibration appeared in region of 962-883 cm^{-1} for **A1**; 987-854 cm^{-1} for **A2**, 1003-862 cm^{-1} for **A3**; 1026-884 cm^{-1} for **A4**; 996-872 cm^{-1} for **A5**, and 997-868 cm^{-1} for **A6** (Table 3).

The NO_2 group stretching vibrations for **A4** are 1671, 1665, 1619 and 1612 cm^{-1}, whereas they are 1639, 1636, 1407 and 1395 for **A5**; this was observed were 1671 and 1639 cm^{-1} [71]. The C=C stretching vibrations observed were 1674, 1670, 1654 and 1628 cm^{-1} for **A1**; 1682, 1674, 1638 and 1629 cm^{-1} for **A2**; 1678, 1677, 1659 and 1649 cm^{-1} for **A3**; 1674, 1656 and 1655 cm^{-1} for **A4**; 1683 1665, 1651 and 1626 cm^{-1} for **A5**, and 1672, 1655, 1643 and 1624 cm^{-1} **A6**. The C=N stretching vibration for **A1** appeared at 1542 and 1526 cm^{-1}; 1575 and 1624 cm^{-1} for **A2**; 1570 and $1550cm^{-1}$ for **A3**; 1566 and 1620 cm^{-1} for **A4**; 1570 and 1521 cm^{-1} for **A5**, and 1564 and 1523 cm^{-1} for **A6,** but it was experimentally observed at 1610 and 1604 m^{-1} [49]. The C=N stretching vibration for 1-(2-nitrobenzoyl)3,5-bis(4-methoxyphenyl)-4,5-dihydro-1 H-pyrazole reported in the range 1608–1531 cm^{-1} [76], however, strong band of C=N was observed around 1628 cm^{-1} and calculated at 1631 cm^{-1} [70].

Table 3. Calculated wave numbers of compounds **A1-A6**.

	A1	**A2**	**A3**	**A4**	**A5**	**A6**
$_{\nu}CH_{3Syn}$	3037	3039	3037	3039	3039	3038
$_{\nu}CH_{3Asy}$	3123, 3094	3125	3123, 3094	3132, 3125,	3124, 3094	3124, 3088
$_{\nu}$C-H $_{(asy)}$	3236, 3222, 3215, 3208, 3196, 3181	3240, 3232, 3220, 3210, 3182	3238, 3184, 3179,	3249, 3228, 3212, 3190	3255, 3246, 3220, 3214	3238, 3245, 3224, 3214
$_{\nu}$C-H_{Sym}	3225, 3212, 3183,	3229, 4214, 3184	3232, 3224	3247, 3215,	3232, 3227, 3213,3203	3236, 3230, 3209
-CH_2- (asy)	3136	3155	3187	3132	3142	3176
-CH_2- (syn)	3084	3086	3097	3077	3085	3082
C-CH_3	1428	1429	1345, 1340	1355, 1343	1353, 1347	1422, 1387
$_{\nu}$C=C	1674, 1670, 1654, 1628	1682, 1674, 1638, 1629	1678, 1677, 1659, 1649	1674,1656, 1655	1683, 1665, 1651, 1626	1672, 1655, 1643, 1624
$_{\nu}$C=N	1542, 1526	1575, 1524	1570, 1550	1566, 1520	1570, 1521	1564, 1523
$_{\nu}$C-F	1247, 1233	1242, 1211, 1206, 1200	1262	-	1223, 1221, 1204	1244, 1245 1202
$_{\nu}NO_2$	-	-	-	1671, 1665, 1619, 1612	1639, 1636, 1407, 1395	-
πC-H	1233, 1221, 1162, 1159, 1148, 1143,	1326, 1311, 1175, 1164, 1159, 1157, 1138	1322, 1312, 1302, 1255, 1244, 1235 1160	1324, 1320, 1289, 1226, 1207, 1203, 1164	1318, 1302, 1289, 1183, 1275, 1264, 1235	1330, 1322, 1246, 1220, 1207, 1178 1154
σC-H	962, 952, 937, 889, 882, 883	978, 967, 888, 863, 860, 854,	1003, 996, 954, 932, 890, 862	1026, 995, 990, 884	996, 951, 942, 872	997, 990, 964, 920, 885, 868

ν, stretching; π, in-plane bending; σ, out plane bending.

3.4. UV-Vis Spectroscopy.

The absorption peaks, percentage of the molecular orbitals involved in the transition, and Oscillator strength (OS) representing a fraction of negatives charges electrons that accomplish a transition calculated (OS > 0.005 were considered) for A1-A6 at B3LYP/6-31G** were displayed in Table SS1. For **A1**, five strong absorptions (i.e., > 0.005 oscillator strength) were calculated at 249.96, 270.4, 273.77, and 281.59 nm arising from the HOMO→LUMO+3 (96%), HOMO-1→LUMO +1 (96%), HOMO→LUMO+1 (85%), HOMO-1→LUMO (68%) and HOMO→LUMO (14%) and HOMO →LUMO (77%) respectively; the longest λ_{max} with highest (OS) was characterized as π-π* transition arising from the HOMO→LUMO (77%). Compound **A2** has four strong absorption peaks at 274.82, 289.33, 293.68, and 300.83 nm, with the longest absorption peak characterized as π-π* transition arising from HOMO→LUMO (87%). For the **A3** molecule, have four strong absorption peaks of 256.33, 270.04, 273.80, and 280.46 nm were observed with the HOMO-1→LUMO+1 (85%) for 256.33 nm, HOMO→LUMO+1 (74%) and HOMO-1→LUMO (21%) for 270.04 nm, HOMO-1→LUMO (60%), HOMO→LUMO+1 (17%) for HOMO→LUMO (15%) for 273.80 nm and HOMO→LUMO (76%) for 280.46 nm which was characterized as π-π* and n-π* transition. Also, for **A4** molecule, 354.14, 359.20, 376.73, and 384.24 nm were four absorption peaks with OS higher than 0.005 arising from the HOMO-1→LUMO+1 (96%), HOMO-1→LUMO (94%) and HOMO→LUMO (65%), HOMO→LUMO+1 (31%) respectively. However, 331.37 nm absorption band of 0.0024 oscillator strength was characterized as n-π* transition.

Moreover, **A5** presented four strong absorption peaks of 327.14, 343.36, 462.00, and 506.97 nm arising from the HOMO-8→LUMO (26%), HOMO-1→LUMO+2 (20%), HOMO-7→LUMO (15%) and HOMO-6→LUMO (13%) for 327.14 nm; HOMO→LUMO+2 (98%) for

343.36 nm; HOMO-1+LUMO+1 (71%) and HOMO-1→LUMO+1 (28%) for 462 nm, and HOMO→LUMO (97%) for 506.97 which was characterized as π-π* transition. For **A6**, there were two strong absorption peaks at 380.56 and 395.59 nm with an oscillator strength value of 0.0231 and 0.0866, arising from the HOMO-3→LUMO (59%) and HOMO→LUMO (76%), respectively. Other four low absorptions at 340.65, 350.73, 378.09 and 448.65 nm were observed arising 0.0021, 0.0021, 0.0030 and 0.0035 OS, respectively (Table 4).

Table 4. Calculated Absorption Peaks, Oscillation Strength, and Molecular Orbitals (MOs) Involved In Transition for **A1-A6.**

A1		
λ_{max} (nm)	Oscillation strength	MO involved in transitions
249.96	0.0070	HOMO -> LUMO+3 96%
254.9	0.0279	HOMO-1 -> LUMO+1 96%
262.58	0.0053	HOMO -> LUMO+2 84%
270.4	0 0.0259	HOMO -> LUMO+1 85%
273.77	0.0778	HOMO-1 -> LUMO 68%
		HOMO -> LUMO 14%
281.59	0.4980	HOMO -> LUMO 77% Triplet
A2		
λ_{max} (nm)	Oscillation strength	MO involved in transitions
263.03	0.0038	HOMO -> LUMO+2 66%
274.82	0.0441	HOMO-1 -> LUMO+1 97%
289.33	0.0558	HOMO -> LUMO+1 71%
		HOMO-1 -> LUMO 26%
293.68	0.0198	HOMO-1 -> LUMO 67% Triplet
		HOMO -> LUMO+1 24%
300.83	0.4864	HOMO -> LUMO 87% Triplet
A3		
λ_{max} (nm)	Oscillation strength	MO involved in transitions
256.33	0.0527	HOMO-1 -> LUMO+1 85%
259.24	0.0016	HOMO -> LUMO+3 59%
		HOMO -> LUMO+2 18%
		HOMO-2 -> LUMO 14%
270.04	0.0479	HOMO -> LUMO+1 74%
		HOMO-1 -> LUMO 21%
273.80	0.0656	HOMO-1 -> LUMO 60%
		HOMO -> LUMO+1 17%
		HOMO -> LUMO 15%
280.46	0.4610	HOMO -> LUMO 76% Triplet
A4		
λ_{max} (nm)	Oscillation strength	MO involved in transitions
331.37	0.0024	HOMO-6 -> LUMO 72%
354.14	0.0158	HOMO-1 -> LUMO+1 96%
359.20	0.0437	HOMO-1 -> LUMO 94%
376.73	0.3496	HOMO -> LUMO 65%
		HOMO -> LUMO+1 31%
389.24	0.0218	HOMO -> LUMO+1 68% Triplet

		HOMO -> LUMO 32%
	A5	
λ_{max} (nm)	Oscillation strength	MO involved in transitions
327.14	0.0103	HOMO-8 -> LUMO 26%
		HOMO-1 -> LUMO+2 20%
		HOMO-7 -> LUMO 15%
		HOMO-6 -> LUMO 13%
343.36	0.0185	HOMO -> LUMO+2 98%
462.00	0.0130	HOMO-1 -> LUMO+1 71% Triplet
		HOMO-1 -> LUMO 28%
471.38	0.0034	HOMO-1 -> LUMO 71% Triplet
		HOMO-1 -> LUMO+1 28%
493.66	0.0042	HOMO -> LUMO+1 98% Triplet
506.97	0.0220	HOMO -> LUMO 97% Triplet
	A6	
λ_{max} (nm)	Oscillation strength	MO involved in transitions
340.65	0.0021	HOMO-2 -> LUMO 88%
350.73	0.0021	HOMO -> LUMO+1 96%
378.09	0.0030	HOMO-4 -> LUMO+1 65%
		HOMO-4 -> LUMO 19%
380.56	0.0230	HOMO-3 -> LUMO 59% Triplet
395.59	0.0866	HOMO -> LUMO 76%
448.65	0.0035	HOMO-1 -> LUMO 94% Triplet

*3.5. Nonlinear Optical Properties of **A1-A6**.*

The nonlinear optical properties (NLO), the strength of molecular interactions, the polarizability (α), hyperpolarizability (β), and the electric dipole moment (μ); were calculated for the studies' compound M1-M6 at DFT B3LY/6-31G** bond on the finite field approach. The total static dipole moment (μ_1), the mean polarizability ($\alpha_\circ$), and the mean first hyperpolarizability ($\beta_\circ$) using x,y, and z components by taking the origin of the Cartesian coordinate system (x, y, z) = (0, 0, 0) at the center of mass of the compounds as defined in the equations:

$$\text{The total static dipole moment } \mu,\ \mu_{total} = (\mu^2_x + \mu^2_y + \mu^2_z)^{1/2}$$

$$\text{The static polarizability } \alpha,\ \alpha = 1/3\ (\alpha_{xx} + \alpha_{yy} + \alpha_{zz})$$

$$\gamma^2 = 1/2(\alpha_{xx} - \alpha_{yy})^2 + (\alpha_{zz} - \alpha_{xx})^2 + 6(\alpha^2_{xx} + \alpha^2_{yy} + \alpha^2_{zz})$$

$$\text{The static hyperpolarizability } \beta,\ \beta_{total} = (\beta^2_x + \beta^2_y + \beta^2_z)^{1/2}$$

$$\beta_{xxx} = [(\beta xxx + \beta xyy + \beta xzz)^2$$

$$\beta_{yyy} = (\beta yyy + \beta yzz + \beta yxx)^2$$

$$\beta_{zzz} = (\beta zzz + \beta zxx + \beta zyy\ )^2$$

The determination of the transference region; thus, the suitability of the molecules for nonlinear optical applications should have the UV-visible absorption above 300 nm, which

might aid the NLO behavior of the molecules [77]. Also, asymmetric polarization as a result of electron donor and acceptor groups in π-electron conjugated molecules has excellent nonlinear optical (NLO) properties for the exploitations in telecommunications, optical signal processing, and optical computing [77,78], thus compounds **A4, A5,** and **A6** should be suitable for optical devices due to their longest absorption wavelengths. The calculated dipole moment, the polarizabilities, and first-order hyperpolarizabilities for six compounds are displayed in Table 5. The calculated values of total dipole moment for **A1-A6** were 4.633, 5.672, 3.780, 7.503, and 6.196 Debye, respectively. However, the dipole moment for **Aa** and 1-(4-(trifluoromethyl)benzyl)-2-(4-(trifluoromethyl)phenyl)-6-methyl-1Hbenzo[d]imidazole were calculated to be 3.3563 and 1.8262 Debye, respectively [49]. Interchanging the fluorine and hydrogen atoms in R_2 and R_3, as seen in **Aa** [49] and **A1**, leads to an increasing dipole moment of **A1** by 1.276 Debye. When R_1, R_2, and R_3 are all fluorine, as shown in **A3**, there was a further increase in dipole moment by 1.0393 and 2.137 Debye compared to **A1** and **Aa**, respectively. The comparative sites of the dipole moment vectors for the molecules could be arranged as follows; **A4** (NO_2, H, H) > **A6** (CF_3, F, HN_2) > **A2** (CF_3, F, H) > **A1** (F, F, H) > **A3** (F, F, F) > **A5** (CF_3, H, NO_2).

Table 5. Calculated Dipole Moment (μ), Mean Polarizability (α), and Hyperpolarizability (β) for **A1-A6.**

Parameter	A1	A2	A3	A4	A5	A6
Dipole moment (μ)						
μ_x	-1.4356	2.8453	3.0327	-6.2749	0.2884	-4.7315
μ_y	0.6625	-1.7787	2.2859	1.7224	2.5941	-2.1818
μ_z	-4.3869	4.5735	-0.1210	-3.7362	1.7333	-3.3538
μ_{total}	4.6331	5.6724	3.7997	7.5034	3.1332	6.1964
Polarizability(α)						
α_{xx}	-147.0444	-187.9682	-157.8857	-183.2786	-206.0275	-201.5767
α_{xy}	-3.9587	-11.7675	7.9620	-3.1463	3.8056	2.9048
α_{yy}	-169.4467	-196.7160	-165.1556	-198.861	-215.8902	-259.6288
α_{xz}	5.4537	-2.0559	6.4428	-0.6815	1.5276	10.2789
α_{yz}	-2.4147	0.4960	3.0343	6.8073	12.2124	-15.8710
α_{zz}	-143.8004	-174.2603	-154.5342	-155.4532	-203.7948	-219.6789
α_{total}	-334.2448	-572.2719	-460.1364	-534.6204	-608.1669	-683.5717
$\alpha \times 10^{-23}$ (esu)	-49.52	-84.81	-68.11	-79.22	-90.13	-10.12
Hyperpolarizability (β)						
βxxx	50.7297	72.2721	2.9909	-284.5629	0.1112	105.4822
βxxy	22.5972	-15.0896	11.9745	-54.0733	-11.1221	-23.3124
βxyy	-30.8905	-43.4346	-15.2288	-23.6272	56.4327	75.3796
βyyy	18.5655	71.8424	20.3888	148.7798	-37.2689	-110.6393
βxxz	-14.3731	14.8525	-5.1579	3.9355	-7.4445	-42.8982
βxyz	-14.5948	14.3947	-7.1148	-3.2729	-22.6849	6.7063
βyyz	-10.5546	1.8201	7.7690	42.4240	14.1705	-62.6236
βxzz	-25.6955	-29.3588	-39.2233	12.9576	74.6939	35.1717
βyzz	4.2868	27.0896	6.8427	1.5417	-23.4386	-33.3705
βzzz	13.1238	-15.4498	13.7381	-7.040	9.1067	35.1178
β_{total}	53.7130	83.853	59.453	312.922	150.444	181.601
$\beta \times 10^{-31}$(esu)	4.64	7.24	5.14	2.703	1.29	1.56

Polarizability (α_o) is directly proportional to absorption wavelength and inversely proportional to the energy value gap; thus, the higher the polarizability value, the longer the λ_{max} and the lower the energy bandgap; this shows that A6 should have the longest λ_{max} because it has the highest polarizability value of -10.12×10^{-23}esu [49]. The polarizability ($\alpha \times 10^{-23}$ (esu)) were estimated to be -49.52, -84.81, -68.11, -79.22, -90.13 and -10.12 for **A1-A6,** respectively; this was calculated to be -43.62 and -2.63 for Aa and 1-(4-

(trifluoromethyl)benzyl)-2-(4-(trifluoromethyl)phenyl)-6-methyl-1Hbenzo[d]imidazole, respectively [49]. As it has been reported, the polarizability (α_o) actual is directly proportional to absorption wavelength and inversely proportional to the energy value gap, and thus, the higher the polarizability value, the longer the λ_{max} and the lower the energy bandgap [49]. The magnitude of the molecular hyperpolarizability β_0 is one of the main factors in a nonlinear optics (NLO) system. Therefore, the hyperpolarizability (β) values were 4.64, 7.24, 5.14, 2.70, 1.29 and 1.56 x 10^{-31} (esu) for compounds **A1-A6**, respectively compared to 79.65 and 25.61 x 10^{-33} (esu) calculated for Aa and 1-(4-(trifluoromethyl)benzyl)-2-(4-(trifluoromethyl)phenyl)-6-methyl-Hbenzo[d]imidazole, respectively [49]. These showed that the hyperpolarizability value of **A1, A2**, and **A3** were nearly 1.5, 1.95, and 1.38 times higher than urea (3.72×10^{-31} esu); thus, **A1-A3** could be a suitable candidate for NLO material.

3.6. Antioxidant and antihypertensive evaluations via Molecular Docking.

The bioactivity of the model compounds was investigated for their antihypertensive and antioxidant properties. Antioxidants are useful food additives to serve as protection against oxidative degradation of foods; they play a very crucial role in the prevention of many degenerative and/or chronic diseases by scavenging reactive oxygen species (oxygen-free radicals), which can initiate the progression of pathologies like atherosclerosis, the decline in immune system decline and even development of abnormal cell growth that can lead to cancer [79]. Imidazole derivatives have been investigated for antioxidant activity, and the results showed they are promising antioxidants [60, 80, 81]. Thus the designed compounds were docked against dehydrogenase inhibitor as APO-liver alcohol dehydrogenase inhibitor, which was downloaded from protein data bank with PDB ID: 5ADH. The results were compared with that of taurine, a well-known antioxidant that protects the hepatic tissue by stabilizing the reactive oxygen species-mediated lipid peroxidation and protein carbonyl formation, osmoregulation, detoxification, and calcium homeostasis, neuromodulation, and cytoprotection [82-84]. It has been reported that this is an inverse relationship between plasma taurine concentrations and fasting plasma sugar (FBS) as well as diabetes complications, indicating taurine has a protective role in the progression of diabetes [85-87].

Hypertension is one of the prevalent cardiovascular diseases, which signifies high-risk factors for metabolic syndrome, renal dysfunction, endothelial dysfunction, coronary artery disease, congestive heart failure, and stroke [88]. It has been reported that imidazole derivatives display the antihypertensive activity [89, 90]; thus, the model compounds were investigated for their antihypertensive activity by docking A1-A6 with an angiotensinogenase. Angiotensinogenase is an aspartic protease protein produced by the kidneys, which involves regulating blood pressure [91]. The antihypertensive protein hydrolase inhibitor was downloaded from the PDB website with PDB ID: 4XX3. The model compounds A1-A6 were docked against 5ADH and 4XX3, respectively, and molecular interactions existing between the docked complexes were examined. Docking simulations were carried out by using AutoDock Tool 1.5.6 and AutoDock Vina, respectively. The receptors/proteins were clean-up and visualization of molecular interaction between receptor and ligand with Pymol and BIOVIA Discovery Studio 2019 as reported in the literature [92-99].

The amino acid residues of the docking complexes of dehydrogenase inhibitor (PDB ID: 5ADH) around the binding pocket interactions with the model compounds revealed that LYS 228 **was** involved in hydrogen bond**;** ILE 296, VAL 203, ARG 47, ILE 296, VAL 203 and ARG 47 in π- Alkyl, and ARG 47 involved in π- cation interactions with **A1.** ARG 369,

ARG 47, VAL 203, and GLY 202 formed hydrogen bonds; PRO 295 and ARG 47 were involved in π- Alkyl, and CYS 46 in π-Sulphur interactions with A2. SER 48 and CYS 46 formed hydrogen bonds; VAL 203 and CYS 46 were involved in π- Sigma; and ARG 47 was involved in π- Cation interactions with A3. ARG47 involved in hydrogen bonding and π- Alkyl interactions**;** VAL 203 formed π- Sigma; and CYS 46 formed π- Sulphur interactions with **A4.** ARG 47 **was** involved in hydrogen bonding, and π- Alkyl interactions; VAL 203 and ILE 269 formed π- Alkyl and π- Sigma interactions, while CYS 46 was involved in π- Sulphur interactions with **A5.** Compound A6 formed a hydrogen bond with VAL 28**;** π- Alkyl interaction with ILE 269 and ARG 47; π- Sigma interaction with ILE 269 and VAL 203; π-Sulphur interaction with CYS 46 (Table 6 and Figure SS1). Taurine was involved in hydrogen bonding with SER 367, ARG 369, and ARG 47 and interacted with VAL 203 and CYS 46 via Van der Waal interactions**.** The docked ligands form stable complexes with dehydrogenase inhibitors which showed binding affinity values of -8.3, -9.0, -8.5, -8.3, -9.5, -8.9, and -3.7 kcal/mol for **A1, A2, A3, A4, A5, A6,** and taurine, respectively (Table 6). The binding affinity calculated for 2-Chloro-4, 5-dimethyl-1-phenyl-1H-imidazole and 2-Chloro-4, 5-dimethyl-1-o-tolyl-1H-imidazole were -5.0 and -5.3 kcal/mol, respectively [60]. This suggested that these compounds could be excellent inhibitors for APO-liver alcohol dehydrogenase inhibitors, thus possessing good antioxidant properties.

Table 6. The predicted binding affinity (**ΔG**) and amino acid interactions of dehydrogenase inhibitor (PDB ID: 5ADH) with **A1-A6** compounds.

Ligand	**ΔG (kcal/ mol)**	**Receptor amino acids with ligands**	**Type of interactions**
A1	-8.3	LYS 228 ILE 296, VAL 203, ARG 47 ARG 47 ASP 223, SER 367	Conventional H-bond π- Alkyl π- Cation π- Fluorine
A2	-9.0	ARG 369, ARG 47, VAL 203, GLY 202 PRO 295, ARG 47 ILE 269, VAL 268 CYS 46	Conventional H-bond π- Alkyl π- Fluorine π- Sulphur
A3	-8.5	SER 48, CYS 46 VAL 203, ARG 47 ARG 47 PRO 295, VAL 292	Conventional H-bond π- Sigma π- Cation π- Fluorine
A4	-8.5	ARG 369, ARG47 ARG 47, ILE 318, PRO 295, PHE 93 VAL 203 HIS 51 CYS 46	Conventional H-bond π- Alkyl π- Sigma π- Cation π- Sulphur
A5	-9.5	ARG 47, ARG 369 VAL 203, ARG 47, ILE 269 ILE 269, VAL 203 ASP 223 CYS 46	Conventional H-bond π- Alkyl π- Sigma π- Fluorine π- Sulphur
A6	-8.9	Val 268 Ile 269, arg 47 Ile 268, val 203 Val 268 Cys 46	Conventional H-bond π- Alkyl π- Sigma π- Fluorine π- Sulphur
Taurine	-3.7	SER 367, ARG 369, ARG 47 VAL 203, CYS 46	Conventional H-bond Van der Waal

The docking results of compounds **A1-A6** with antihypertensive protein hydrolase (PDB ID: 4XX3) to reveal the antihypertensive properties showed that SER107, SER296, and THR 151 involved in hydrogen bond; LEU187, ALA295, ALA188 and PRO 184 involved in π-Alkyl; PHE 190 and TYR 149 in π-π- T-shaped; and ASP104 and GLY106 in π-Fluorine interactions with **A1**. TYR 297 and SER 296 formed hydrogen bonds; MET 369, ALA 295, VAL 193, VAL 102, and ASP 104 were involved in π-Alkyl; and GLY 294 in π-Fluorine interactions with **A2.** THR 151 in π-Donor H-bond; PRO 184, TYR 297, and ALA 295 in π-Alkyl; ALA 295 and THR 151 in π-Sigma bond; and PRO 184, GLM 85, GLY 294, ASP104 in π-Fluorine with compound **A3**. The interactions of the receptor with **A4** showed that SER296, TYR 297, and TYR 86 in hydrogen bond; VAL 193, TYR149, PHE 185, and VAL 102 in π-Alkyl; ALA 295 and THR 151 in π-Sigma bond; and PHE 190 in π- π Stacked interactions. TRP 267, GLN 201, and SER 150 in hydrogen bond; SER 107 and GLY 106 involved in π-Donor H-bond; ALA 380, ALA295, ILE 371, MET 369, and PRO 372 in π-Alkyl; GLY 106 and VAL 266 in Amide- π Stacked; and ASP 292 in π- Anion interactions with **A5.** ASP 104, SER 296, and TYR 297 formed hydrogen bonds; ALA380, PHE 190, VAL 193, VAL 102, and TYR 145 were involved in π-Alkyl; ASP 104 and GLY 294 formed π-Fluorine; ALA 295 formed π-Sigma; TYR 149 involved in π- π T-shaped; and MET 369 and ASP 292 involved in π- sulfur interactions with compound **A6** (Table 7 and Figure SS2). Docking results of the compounds with hydrolase inhibitor (PDB ID: 4XX3) showed that binding affinities. A1-A6 ranged from -9.2 to -10.0 kcal/mol (Table 7). These were higher than the binding affinity calculated for similar compounds; (1-(4-methoxyphenyl)-4,5-dimethyl-1H-imidazole-2-yl acetate and 1-(4-bromophenyl)-4,5-dimethyl-1H-imidazole-2-yl acetate with binding affinity values of -6.4 and -6.7 kcal/mol, respectively [6].

Table 7. The predicted binding affinity (**ΔG**) and amino acid interactions of antihypertensive protein hydrolase (PDB ID: 4XX3) with A1-A6 compounds.

Ligand	ΔG (kcal/mol)	Receptor amino acids with ligands	Type of interactions
A1	-9.2	SER107, SER296 THR 151 LEU187, ALA295, ALA188, PRO 184 PHE 190, TYR 149 ASP104, GLY106	Conventional H-bond π-Donor H-bond π-Alkyl π- π T-shaped π-Fluorine
A2	-9.6	TYR 297 SER 296 MET 369, ALA 295, VAL 193, VAL 102, ASP 104 GLY 294	Conventional H-bond Carbon H-bond π-Alkyl π-Fluorine
A3	-9.4	THR 151 PRO 184, TYR 297, ALA 295 ALA 295, THR 151 PRO 184, GLM 85, GLY 294, ASP104	π-Donor H-bond π-Alkyl π-Sigma bond π-Fluorine
A4	-9.8	SER296, TYR 297, TYR 86V VAL 193, TYR149, PHE 185, VAL 102 ALA 295, THR 151 PHE 190	Conventional H-bond π-Alkyl π-Sigma bond π- π Stacked
A5	-10.1	TRP 267, GLN 201, SER 150 SER 107, GLY 106 ALA 380, ALA295, ILE 371, MET 369, PRO 372 GLY 106, VAL 266 ASP 292	Conventional H-bond π-Donor H-bond π-Alkyl Amide- π Stacked π- Anion
A6	-10.0	ASP 104, SER 296, TYR 297 ALA380, PHE 190, VAL 193, VAL 102, TYR 145 ASP 104, GLY 294 ALA 295 TYR 149 MET 369, ASP 292	Conventional H-bond π-Alkyl π-Fluorine π-Sigma π- π T-shaped π- sulphur

This suggested that the model compounds **A1-A6** could be outstanding inhibitors for antihypertensive protein hydrolase inhibitors and thus possess good antihypertensive properties.

4. Conclusions

The molecular parameters, electrostatic potential, nonlinear optical properties, antioxidant and antihypertensive properties of six model compounds of 1-benzyl-2-phenyl-1*H*-benzimidazole derivatives were reported experimentally. The calculated geometries, electron-donating and accepting power potential energy, and charge distribution in terms of MEP analysis were discussed. The electron-donating power (ω^-) showed that **A1, A2,** and **A3** could be good electron donors, while electron-accepting power (ω^+) revealed the tendency of **A4** and **A5** to be good electron acceptors in line with μ and ω values. The MEP analysis shows the nitrogen atom of the imidazole ring to be a center of electrophilic attacks. The magnitude of the molecular hyperpolarizability suggested that compounds **A1 –A3** have good nonlinear optical properties that could be explored as a candidate for NLO materials. The docking results showed that these compounds could be excellent antioxidant and antihypertensive properties.

Funding

This research did not receive any specific grant from funding agencies in the public, commercial, or not-for-profit sectors.

Acknowledgments

We are grateful to the Department of Pure and Applied Chemistry, Ladoke Akintola University of Technology, Ogbomoso, for the computational resources and Mrs. E.T. Oyebamiji and Miss Priscilla F. Oyebamiji for their assistance in the course of this study.

Conflicts of Interest

The authors declare no conflict of interest.

References

1. Santos, J.; Mintz, E.A.; Zehnder, O.; Bosshard, C.; Bu, X.R.; Gunter, P. New class of imidazoles incorporated with thiophenevinyl conjugation pathway for robust nonlinear optical chromophores. *Tetrahedron Lett.* **2001**, *42*, 805–808, https://doi.org/10.1016/S0040-4039(00)02143-2.
2. Sharma, D.; Narasimhan, B.; Kumar P, Judge, V.; Narang, R.; De Clercq, E.; Balzarini, J. Synthesis, antimicrobial and antiviral evaluation of substituted imidazole derivatives. *Eur. J. Med. Chem.* **2009**, *44*, 2347-2353, https://doi.org/10.1016/j.ejmech.2008.08.010.
3. Johnson, T.O.; Adegboyega, A.A.; Iwaloye, O.; Eseola, O.A.; Plass, W.; Afolabi, B.; Rotimi, D.; Ahmed, E.I.; Albrakati, A.; Batiha, G.E.; Adeyemi, O.S. Computational study of the therapeutic potentials of a new series of imidazole derivatives against SARS-CoV-2. *J. Pharmacol. Sci.* **2021,** *147*, 62-71, https://doi.org/10.1016/j.jphs.2021.05.004.
4. Laufer, S.A.; Zimmermann, W.; Ruff, K.J. Tetrasubstituted imidazole inhibitors of cytokine release: probing substituents in the N-1 position. *J. Med. Chem.* **2004**, *47*, 6311-6325, https://doi.org/10.1021/jm0496584.
5. Wolkenberg, S.E.; Wisnoski, D.D.; Leister, W.H.; Wang, Y.; Zhao, Z.; Lindsley, C.W. Efficient synthesis of imidazoles from aldehydes and 1,2-diketones using microwave irradiation. *Org. Lett.* **2004**, *6*, 1453-1456, https://doi.org/10.1021/ol049682b.
6. Hossain, M.; Thomas, R.; Mary, Y.S.; Resmi, K.S.; Armakovic, S.; Armakovic, S.J.; Nanda, A.K.; Vijayakumar, G.; Van Alsenoy, C. Understanding reactivity of two newly synthetized imidazole derivatives

by spectroscopic characterization and computational study. *J. Mol. Stru.* **2018**, *1158*, 176-196, https://doi.org/10.1016/j.molstruc.2018.01.029.
7. Ionic Liquids in Synthesis.*Wasserscheid, P.; Welton, T. (Eds.)* **2008**, *2nd Ed*, Wiley-VCH, Weinheim, http://dx.doi.org/10.1002/9783527621194.ch1.
8. Jin, C.H.; Krishnaiah, M.; Sreenu, D.; Subrahmanyam, V.B.; Rao, K.S.; Lee, H.J.; Park, S.J.; Park, H.J.; Lee, K.; Sheen, Y.Y.; Kim, D.K. Discovery of N-((4-([1,2,4]triazolo[1,5a]pyridine-6-yl)-5-(6-methylpyridin-2-yl)-1H-imidazole-2-yl) methyl)-2-fluoroaniline (EW-7197): a highly potent, selective and orally bioavailable inhibitor of TGF-b type I receptor kinase as cancer immunotherapeutic/antifibrotic agent. *J. Med. Chem.* **2014**, *57*, 4213-4238, https://doi.org/10.1021/jm500115w.
9. Zhang, L.; Peng.; Damu, G.L.; Geng, R.X.; Zhou, C.H. Comprehensive review in current developments of imidazole based medicinal chemistry. *Med. Res. Rev*. **2014**, *34*, 340-437, https://doi.org/10.1002/med.21290.
10. Rohring, U.F.; Majjigapu, S.R.; Chambon, M. *et al*. Detailed analysis and follow up studies of a high throughput screening for indoleamine 2,3-dioxygenase 1(IDO1) inhibitors. *Eur. J. Med. Chem*. **2014**, *84*, 284-301, https://doi.org/10.1016/j.ejmech.2014.06.078.
11. Choi, J.Y.; Plummer, M.S.; Starr, J.; Desbonnet, C.R.; Soutter, H.; Chang, J.; Miller, J.R.; Dillman, K.; Miller, A.A.; Roush, W.R. Structure guided development of novel thymidine mimetics targeting pseudomonas aeruginosa thymidylate kinase, from hit to lead generation. *J. Med. Chem.* **2012**, *55*, 852-870, https://doi.org/10.1021/jm201349f.
12. Yurttas, L.; Duran, M.; Demirayak, S.; Gençer, H.K.; Tunalı, Y. Synthesis and initial biological evaluation of substituted 1-phenylamino-2-thio-4,5-dimethyl-1Himidazole derivatives. *Bioorg. Med. Chem. Lett.* **2013**, *23*, 6764-6768, https://doi.org/10.1016/j.bmcl.2013.10.024.
13. Ucucu, U.; Karaburun, N.G.; Isikdag, I. Synthesis and analgesic activity of some 1-benzyl-2-substituted-4,5-diphenyl-1H-imidazole derivatives. *Farmaco.* **2001**, *56*, 285–290, https://doi.org/10.1016/s0014-827x(01)01076-x.
14. Verma, A.; Joshi S.; Singh, D. Imidazole: Having versatile biological activities. *J. Chem.* **2013,** *2013*, https://doi.org/10.1155/2013/329412.
15. Turkey, R. H.; Kubba, A.A.M. Synthesis, characterization and antibacterial activity of new 5-ethoxy-2-mercapto benzimidazole derivatives. *J. Pharm. Res.* **2016**, *10*, 814-824.
16. Patil, A.; Ganguly, S.; Surana, S. A systematic review of benzimidazole derivatives as an antiulcer agent. *Rasayan J. Chem*. **2008**, *1*, 447-460.
17. Salahuddin, Shaharyar, M.; Mazumder, A. Benzimidazoles: A biologically active compounds. *Arabian J. Chem*. **2017**, *10*, S157–S173, https://doi.org/10.1016/j.arabjc.2012.07.017.
18. Mavrova, A.T.; Vuchev, D.; Anichina, K..; Vassilev, N. Synthesis, antitrichinnellosis and antiprotozoal activity of somenovel thieno[2,3-d]pyrimidin-4(3H)-ones containing benzimidazole ring. *Eur. J. Med. Chem*. **2010**, *45*, 5856-5861, https://doi.org/10.1016/j.ejmech.2010.09.050.
19. Chen, J.; Wang, Z.; Li, C-M.; Lu, Y.; Vaddady, P.K.; Melbohm, B.; Dalton, J.T.; Miller, D.D.; Li, W. Discovery of novel 2-aryl-4-benzoyl-imidazoles targeting the colchicines binding site in tubulin as potential anticancer agents. *J. Med. Chem*. **2010**, *53*, 7414–7427, https://doi.org/10.1021/jm100884b.
20. Al-kazweeny, R.; Muhi-eldeen, Z.A.; Al-kaissi, E.; Al-tameemi, S.; Tayeh, S.S.; Al-hussenini, J. Designs, synthesis, structural elucidation and antimicrobial evaluation of various derivatives of 2-mercaptobenzimidazole as possible antimicrobial agents. *Int. J. Med. Res. Health Sci*. **2020**, *9*, 1-13.
21. Achar, K.C.S.; Hosamani, K.M.; Seetharamareddy, H.R. In-vivo analgesic and anti-inflammatory activities of newly synthesized benzimidazole derivatives. *Eur. J Med Chem.* **2010**, *45*, 2048-2054, https://doi.org/10.1016/j.ejmech.2010.01.029.
22. Datar, P.A.; Limaye, S.A. Design and synthesis of Mannich bases as benzimidazole derivatives as analgesic agents. *AntiInflamm AntiAllergy Agents Med. Chem.* **2015,** *14*, 35-46, https://doi.org/10.2174/1871523014666150312164625.
23. Gellis, A.; Kovacic, H.; Boufatah, N.; Vanelle, P. Synthesis and cytotoxicity evaluation of some benzimidazole-4,7-diones as bioreductive anticancer agents. *Eur. J. Med. Chem.* **2008**, *43*, 1858-1864, https://doi.org/10.1016/j.ejmech.2007.11.020.
24. Tahlan, S.; Kumar, S.; Narasimhan, B. Pharmacological signifcance of heterocyclic 1H-benzimidazole scafolds: A review. *BMC Chemistry* **2019**, *13*, 101, https://doi.org/10.1186/s13065-019-0625-4.
25. Ghoneim, K.M.; Essawi, M.Y.H.; Mohamed, M.S.; Kamal, A.M.; El-Megid, R.M.A. Synthesis of 2-[(4-amino or 2,4-diaminophenyl)sulfonyl] derivatives of benzimidazole, benzothiazole and 6-methyluracil as potential antimicrobial agents. *Ind. J. Chem.* **1998**, *37B*, 904-911.

26. Torres-Gomez, H.; Hernandez-Nunez, E.; Leon-Rivera, I. *et al*. Design, synthesis and in vitro antiprotozoal activity of benzimidazole-pentamidine hybrids. *Bioorg. Med. Chem. Lett.* **2008**, *18*, 3147-3151, https://doi.org/10.1016/j.bmcl.2008.05.009.
27. Gowda, J.; Khadar, A.M.A.; Kalluraya, B.; Kumari, N.S. Microwave assisted synthesis of 1,3,4-oxadiazoles carrying benzimidazole moiety and their antimicrobial properties. *Ind. J. Chem.* **2010**, *49B*, 1130-1134.
28. Bu, X.R.; Li, H.; Derveer, D.V.; Mintz, E.A. A novel approach to synthesis of tricyanovinylthiophene for heterocyclic imidazole nonlinear optical chromophores. *Tetrahedron Lett*. **1996**, *37*, 7331–7334, https://doi.org/10.1016/0040-4039(96)01638-3.
29. Chao, H.; Ye, B.H.; Zhang, Q.L.; Ji, L.N. A luminescent pH sensor based on a diruthenium(II) complex: "off-on-off" switching via the protonation/deprotonation of an imidazole-containing ligand. *Inorg Chem Commun* **1999**, *2*, 338–340, https://doi.org/10.1016/S1387-7003(99)00089-1.
30. Moylan, C.R.; Miller, R.D.; Twieg, R.J.; Betterton, K.M.; Lee, V.Y.; Matray, T.J.; Nguyen, C. Synthesis and nonlinear optical properties of donor-acceptor substituted triaryl azole derivatives. *Chem. Mater.* **1993,** *5*, 1499–1508, https://doi.org/10.1021/cm00034a021.
31. Kirk, K.L. Fluorine in medicinal chemistry: recent therapeutic application of fluorinated small molecules. *J. Fluor. Chem.* **2006**, *127*, 1013–1029, https://doi.org/10.1016/j.jfluchem.2006.06.007.
32. Koch, R.; Finnerty, J.J.; Bruhn, T. Theoretical study on the nonlinear optical properties of phenylenes and influencing factors. *J. Phys. Org. Chem.* **2008**, *21*, 954–962, https://doi.org/10.1002/poc.1405.
33. Ye, G.; Henry, W.P.; Chen, C.; Zhou, A.; Pittman Jr., C.U. Push–pull alkenes by reacting N,N′-dimethyl cyclic ketene N,N′-acetals with isocyanates: synthesis, structures, and reactivities. *Tetrahedron Lett.* **2009**, *50*, 2135–2139, https://doi.org/10.1016/j.tetlet.2009.02.160.
34. Lee, C.M.; Jeong, H.J.; Lim, S.T.; Sohn, M.H.; Kim, D.W. Synthesis of iron oxide nanoparticles with control over shape using imidazolium-based ionic liquids. *ACS Appl. Mater. Interfaces* **2010**, *2*, 756–759, https://doi.org/10.1021/am900769x.
35. Jayabharathi, J.; Thanikachalam, V.; Perumal, M.V., Physicochemical and solvatochromic analysis of an imidazole derivative as NLO material. *Spectrochimica Acta Part A:Molec. and Biomolec. Spectrosc*. **2012**, *85*, 31–37, https://doi.org/10.1016/j.saa.2011.08.060.
36. Wiest, O.; Houk, K.N. Density functional theory calculations of pericyclic reaction transition structures. In: *Nalewajski, R.F. (eds) Density Functional Theory IV. Topics in Current Chemistry, vol 183*, Springer, Berlin, Heidelberg, https://doi.org/10.1007/3-540-61131-2_1.
37. Glukhovtsev, M.N.; Bach, R.D.; Pross, A.; Radom, L. The performance of B3-LYP density functional theory in describing SN2 reactions at saturated carbon. *Chem. Phy. Lett.* **1996**, *260*, 558-564, https://doi.org/10.1016/0009-2614(96)00923-2.
38. Sadhukhan, S.; Muñoz, D.; Adamo, C.; Scuseria, G.E. Predicting proton transfer barriers with density functional methods. *Chem. Phys. Lett.* **1999**, *306*, 83-87, https://doi.org/10.1016/S0009-2614(99)00442-X.
39. Semire, B.*;* Mutiu, O.; Oyebamiji, K.A. *Ab initio* and DFT Methods on NMR, IR and Reactivity Indices of Indol-3-carboxylate and Indazole-3-carboxylate Derivatives of Cannabinoids: Comparative Study. *J. Phys. Theo. Chem.* **2017**, *13*, 353-377.
40. Hiteshi, T.; Tanmoy, C.; Vandana, S. A Brief Review on Importance of DFT In Drug Design. *Res Med Eng Sci*. **2019**, *7*, RMES.000668, 791-795.
41. Deng, W.Q.; Sun, L.; Huang, J.D.; Chai, S.; Wen, S.H.; Han, K.L. Quantitative prediction of charge mobilities of pi-stacked systems by first-principles simulation. *Nat. Protoc*. **2015**, *10*, 632-642, https://doi.org/10.1038/nprot.2015.038.
42. Reig, M.; Bagdziunas, G.; Volyniuk, D.; Grazulevicius, J.V.; Velasco, D. Tuning the ambipolar charge transport properties of tricyanovinyl-substituted carbazolebased materials, *Phys. Chem. Chem. Phys.* **2017**, *19*, 6721-6730, https://doi.org/10.1039/C6CP08078B.
43. Zhan, X.; Shi, H.; Liu, H.; Lee, J.Y. Applying strong external electric field to thiophene-based oligomers: a promising approach to upgrade semiconducting performance. *J. Comput. Chem*. **2017**, *38*, 304-311, https://doi.org/10.1002/jcc.24684.
44. Semire, B.; Oyebamiji, AK.; Odunola, O.A. Tailoring of Energy Levels in (2Z)-2-cyano-2-[2-[(E)-2-[2-[(E)-2-(p-tolyl)vinyl]thieno[3,2-b]thiophen-5-yl]vinyl]pyran-4-ylidene]acetic acid Derivatives via Conjugate Bridge and Fluorination of Acceptor units for Effective D-π-A Dye-Sensitized Solar Cells: DFT-TDDFT Approach. *Res. Chem. Intermed.* **2017,** *43*, 1863–1879, http://dx.doi.org/10.1007%2Fs11164-016-2735-0.

45. Afolabi, S.A.; Semire, B.; Akiode, O.K.; Afolabi, T.A.; Adebayo, G.A.; Idowu, M.A. Design and theoretical study of phenothiazine-based low bandgap dye derivatives as sensitizers in molecular photovoltaics. *Opt. Quant. Electro* **2020,** *52*, 476, https://doi.org/10.1007/s11082-020-02600-5.
46. Afolabi, S.A.; Semire, B.; Idowu, M.A. Electronic and optical properties' tuning of phenoxazine-based D-A2-π-A1 organic dyes for dye-sensitized solar cells. DFT/TDDFT investigations *Heliyon* **2021,** *7*, e06827, https://doi.org/10.1016/j.heliyon.2021.e06827.
47. Semire, B.; Oyebamiji, A.K.; Odunola, O.A. Electronic Properties' Modulation of D-A-A via Fluorination of 2-Cyano-2-pyran-4-ylidene-Acetic Acid Acceptor Unit for Efficient DSSCs: DFT-TDDFT Approach. *Scientific African* **2020**, *7*, e00287, https://doi.org/10.1016/j.sciaf.2020.e00287.
48. He, Y.; Huang, Y.; Li, J.; Pang, X.; Yang G. Unveiling photophysical properties of phenanthro[9,10-d]imidazole derivatives for organic light-emitting diodes. *Org. Electron.* **2020**, *50*, 220-227, https://doi.org/10.1016/j.orgel.2017.08.002.
49. Manikandan, I.; Perumal, M.V.; Jayamoorthy, K. Synthesis, Characterization, Physico-Chemical and DFT Studies of Potential Organic NLO Materials: Experimental and Theoretical Combined Study. *Silicon* **2018**, *11*, 425–435, https://doi.org/10.1007/s12633-018-9837-9.
50. Spartan Student user's guide **2019**. *Wavefunction, Inc*, Irvine, CA 92612, USA.
51. Hehre, W.J.; Radom, L.; Schleyer, P.V.R.; Pope, J.A. Ab initio molecular Orbital Theory. Wiley, New York, **1986**.
52. Becke, A.D. Density-functional thermochemistry. III. The role of exact exchange. *J. Chem. Phys*. **1993**, *98*, 5648, https://doi.org/10.1063/1.464913.
53. Lee, C.; Yang, W.; Parr, R.G. Development of the Colle-Salvetti correlation-energy formula into a functional of the electron density. *Phys. Rev. B* **1988**, *37*, 785-789, https://doi.org/10.1103/PhysRevB.37.785.
54. Spartan'14 **2014**. *Wavefunction, Inc*, Irvine, CA 92612, USA.
55. Merrick, J.P.; Moran, D.; Radom, L. An Evaluation of Harmonic Vibrational Frequency Scale Factors. *J. Phys. Chem. A* **2007**, *111*, 11683-11700, https://doi.org/10.1021/jp073974n.
56. Delgado-Montiel, T.; Baldenebro-Lopez, J.; Soto-Rojo, R.; Glossman-Mitnik, D. Quantum chemical study of the effect of π-bridge on the optical and electronic properties of sensitizers for DSSCs incorporating dioxythiophene and thiophene units. *Theor. Chem. Acc.* **2016,** *135*, 235, https://link.springer.com/article/10.1007/s00214-016-1989-3.
57. Delgado-Montiel, T.; Baldenebro-Lopez, J.; Soto-Rojo, R.; Glossman-Mitnik, D. Theoretical study of the effect of π-bridge on optical and electronic properties of carbazole-based sensitizers for DSSCs. *Molecules* **2020**, *25*, 3670, https://doi.org/10.3390/molecules25163670.
58. Parr, R.G.; Szentpaly, L.; Liu, S. Electrophilicity index. *J. Am. Chem. Soc*. **1999**, *121*, 1922–1924, https://doi.org/10.1021/ja983494x.
59. Gazquez, J.L.; Cedillo, A.; Vela, A. Electrodonating and electroaccepting powers. *J. Phys. Chem*. **2007**, *111*, 1966–1970, https://doi.org/10.1021/jp065459f.
60. Smitha, M.; Mary, Y.S.; Hossain, M,; Resmi, K.S.; Armakovic, S.; Armakovic, S.J.; Pavithran, R.; Nanda, A.K.; Van Alsenoy, C. Two novel imidazole derivatives Combined experimental and computational study. *J. Mol. Struct.* **2018**, *1173*, 221-239, https://doi.org/10.1016/j.molstruc.2018.06.110.
61. Benzon, K.B.; Varghese, H.T.; Panicker, C.Y.; Pradhan, K.; Tiwary, B.K.; Nanda, A.K.; Van Alsenoy, C. Spectroscopic investigation (FT-IR and FT-Raman), vibrational assignments, HOMO-LUMO, NBO, MEP analysis and molecular docking study of 2-(4-hydroxyphenyl)-4,5-dimethyl-1H-imidazole 3-oxide, *Spectrochim. Acta Part A* **2015**, *146*, 307-322, https://doi.org/10.1016/j.saa.2015.03.063.
62. Oliva, M.M.; Rodriguez, S.; Casado, J.; Lopez Navarrete, J.T.; Seixas de Melo, J.S.; Rozen, S. Optical properties of [all]-S,S-dioxide oligothiophenes. *Port Electrochim Acta* **2009**, *27*, 531–537, http://dx.doi.org/10.4152/pea.200905533.
63. Liu, G.; Yu, J. Theoretical study on the structure, vibrational frequency and thermodynamic properties of 2,3,7,8-tetrachlorinated dibenzo-p-dioxin. *J. Mol. Struct.: THEOCHEM* **2005**, *717*, 15–19, http://dx.doi.org/10.1016/j.theochem.2004.09.053.
64. Semire, B.; Odunola, O.A.; Adejoro, I.A. Structural and electronic properties of 4H-cyclopenta[2,1-b,3;4-b′]dithiophene S-oxide (BTO) derivatives with an S, S=O, O, SiH_2, or BH_2 bridge: semi-empirical and DFT study. *J. Mol. Model*. **2012**, *18*, 2755–2760, https://doi.org/10.1007/s00894-011-1291-1.
65. Kim, B.-G.; Zhen, C.-G.; Jeong, E.J.; Kieffer, J.; Kim, J. Organic Dye Design Tools for Effi cient Photocurrent Generation in Dye-Sensitized Solar Cells: Exciton Binding Energy and Electron Acceptors. *Adv. Funct. Mater*. **2012**, *22*, 1606–1612, https://doi.org/10.1002/adfm.201101961.

66. Kim, B.-G.; Chung, K.; Kim, J. Molecular Design Principle of All-organic Dyes for Dye-Sensitized Solar Cells. *Chem. Eur. J.* **2013**, *19*, 5220-5230, https://doi.org/10.1002/chem.201204343.
67. Semire, B.; Oyebamiji, A.; Odunola, O.A. Design of (2Z)-2-cyano-2-[2-[(E)-2-[5-[(E)-2-(4-dimethylaminophenyl)vinyl]-2-thienyl]vinyl]pyran-4-ylidene]acetic acid derivatives as D-p-A dye sensitizers in molecular photovoltaics: A density functional theory approach. *Res. Chem. Intermed* **2016,** *42*, 4605-4619, https://doi.org/10.1007/s11164-015-2303-z.
68. Omri, N.; Yahyaoui, M.; Banani, R.; Messaoudi, S.; Moussa, F.; Abderrabba, M. Ab-initio HF and density functional theory investigations on the synthesis mechanism, conformational stability, molecular structure and UV spectrum of N0-Formylkynurenine. *J. Theor. Comput. Che*m. **2016**, *15*, 1650006, https://doi.org/10.1142/S0219633616500061.
69. Kosar, B.; Albayrak, C. Spectroscopic investigations and quantum chemical computational study of (E)-4-methoxy-2-[(p-tolylimino)methyl]phenol. *Spectrochim Acta Part A* **2011**, *78*,160-167, https://doi.org/10.1016/j.saa.2010.09.016.
70. Bharathi, R.; Santhi, N. Combined experimental and theoretical studies on molecular structures, spectroscopy of 4-(3-(2-amino-3,5-dibromophenyl)-1-(benzoyl)-4,5-dihydro-1H-pyrazol-5-yl)benzonitriles through NBO, FT-IR, HOMO-LUMO and NLO analyses. *J. Theor. Comput. Chem.* **2017**, *16*, 1750057, https://doi.org/10.1142/S0219633617500572.
71. Bouzayen, N.; Mbarek, M.; Alimi, K. Solvent effects on optical and electronic properties of carbazole benzothiazole based bipolar compound: TD-DFT/PCM approach. *Mor. J. Chem* **2015,** *3*, 28–39, https://doi.org/10.48317/IMIST.PRSM/morjchem-v3i1.2259.
72. Kumar, M.D.; Rajesh, P.; Dharsini, R.P.; Inban, M.E. Molecular geometry, NLO, MEP, HOMO-LUMO and mulliken charges of substituted piperidine phenyl hydrazines by using density functional theory. *Asian J. Chem.* **2020**, *32*, 401–407, http://dx.doi.org/10.14233/ajchem.2020.22444.
73. Raftani, M.; Abram, T.; Azaid, A.; Kacimi, R.; Bennani, M.N.; Bouachrine, M. Theoretical study of new conjugated compounds with a low bandgap for bulk heterojunction solar cells: DFT and TD-DFT study. *Mater. Today: Proc.* **2021**, *45*, 7334–7343, https://doi.org/10.1016/j.matpr.2020.12.1228.
74. Semire, B.; Adewale, B.A. Density Functional Theory (DFT) Study on Structural and Electronic Properties of Disperse Dyes Derived from 2-Amino-4-Trifluoromethylbenzothiazole and N, N-Alkylanilines. *Int. J. Appl. Chem.* **2013**, *9*, 151-163.
75. Anbu, V.; Vijayalakshmi, K.A. Quantum Chemical Studies on the Spectroscopic, Electronic Structural and Nonlinear Properties of an Organic N-Methyl-N-(2,4,6-Trinitrophenyl) Nitramide Energetic Molecul. *J. Curr. Phys. Chem.* **2019**, *9*, 5-21, https://doi.org/10.2174/1877946809666190218154806.
76. Evecen, M.; Tanak, H.; Tinmaz, F.; Dege, N.; Ilhan, O.I. Experimental (XRD, IR and NMR) and theoretical investigations on 1-(2-nitrobenzoyl)3,5-bis(4 -methoxyphenyl)-4,5-dihydro-1 H-pyrazole. *J. Mol. Struct.* **2016**, *1126*, 117-126, https://doi.org/10.1016/j.molstruc.2016.01.069.
77. Srinivasan, P.; David Stephen, A. DFT and Bader's AIM analysis of 2, 5, diphenyl-1, 3, 4-oxadizole molecule: A organic light emitting diode (OLED). *J .Theor. Comput. Chem.* **2015**, *14*, 1550038, https://doi.org/10.1142/S0219633615500388.
78. Jin, Z.M.; Zhao, B.; Zhou, W.; Jin, Z. X-ray powder diffraction analysis of a nonlinear optical material o–chlorobenzol–benzoyl thiourea. *Power Diffra*. **1997**, *12*, 47-48, https://doi.org/10.1017/S0885715600009428.
79. Behl, C. Amyloid beta-protein toxicity and oxidative stress in Alzheimer's disease. *Cell Tissue Res*. **1997**, *290*, 471-480, https://doi.org/10.1007/s004410050955.
80. Naika, N.; Kumar, H.V.; Rangaswamy, J.; Harini, S.T.; Umeshkumar, T.C. Three component one pot synthesis of 5-Substituted 1-Aryl-2,3-diphenyl imidazoles: a novel class of promising antioxidants. *J. Appl. Pharmaceut. Sci*. **2012**, *2*, 067-074, http://dx.doi.org/10.7324/JAPS.2012.21112.
81. Singh, P.; Kumar, R..; Tiwari, S.; Khanna, R.S.; Tewari, A.K.; Khanna, H.D. Docking, synthesis and evaluation of antioxidant activity of 2,4,5-triaryl imidazole. *Clin. Med. Biochem*. **2015**, *1*, 105, http://dx.doi.org/10.4172/2471-2663.1000105.
82. Bouckenooghe, T.; Remacle, C.; Reusens, B. Is taurine a functional nutrient? *Curr. Opin. Clin. Nutr. Metab. Care*. **2006**, *9*, 728–733, https://doi.org/10.1097/01.mco.0000247469.26414.55.
83. Sirdah, M.M. Protective and therapeutic effectiveness of taurine in diabetes mellitus: a rationale for antioxidant supplementation. *Diab. Metab. Syndr.* **2015**, *9*, 55–64, https://doi.org/10.1016/j.dsx.2014.05.001.
84. Murakami S. Role of taurine in the pathogenesis of obesity. *Mol. Nutr. Food. Res.* **2015**, *59*, 1353–1363, https://doi.org/10.1002/mnfr.201500067.

85. Franconi, F.; Bennardini, F.; Mattana, A.; Miceli, M.; Ciuti, M.; Mian, M.; Gironi, A.; Anichini, R.; Seghieri, G. Plasma and platelet taurine are reduced in subjects with insulin-dependent diabetes mellitus: effects of taurine supplementation. *Am. J. Clin. Nutr.* **1995**, *61*, 1115-1119, https://doi.org/10.1093/ajcn/61.4.1115.
86. Sak, D.; Erdenen, F.; Müderrisoglu, C.; Altunoglu, E.; Sozer, V.; Gungel, H.; Guler, P.A.; Sak, T.; Uzun, H. The relationship between plasma taurine levels and diabetic complications in patients with type 2 diabetes mellitus. *Biomolecules* **2019**, *9*, 96, https://doi.org/10.3390/biom9030096.
87. Maleki, V.; Mahdavi, R.; Hajizadeh-Sharafabad, F.; Alizadeh, M. The effects of taurine supplementation on oxidative stress indices and inflammation biomarkers in patients with type 2 diabetes: a randomized, double-blind, placebo-controlled trial. *Diabetol. Metab. Syndr*. **2020**, *12*, 9, https://doi.org/10.1186/s13098-020-0518-7.
88. Kümmerle, A.E.; Raimundo, J.M.; Leal, C.M.; da Silva, G.S.; Balliano, T.L.; Pereira, M.A.; de Simone, C.A.; Sudo, R.T.; Zapata-Sudo, G.; Fraga, C.A.M.; Barreiro, E. Studies towards the identification of putative bioactive conformation of potent vasodilator arylidene N-acylhydrazone derivatives. *Eur. J. Med. Chem.* **2009**, *44*, 4004- 4009, https://doi.org/10.1016/j.ejmech.2009.04.044.
89. Szabo, B. Imidazoline antihypertensive drugs: a critical review on their mechanism of Action. *Pharmacol. Ther*. **2002**, *93*, 1-35, https://doi.org/10.1016/S0163-7258(01)00170-X.
90. Navarrete-Vazquez, G.; Hidalgo-Figueroa, S.; Torres-Piedra, M.; Vergara-Galicia, J.; Rivera-Leyva, J.C.; Estrada-Soto, S.; Leon-Rivera, I.; Aguilar-Guardarrama, B.; Rios-Gomez, Y.; Villalobos-Molina, R.; Ibarra-Barajas, M. Synthesis, vaso- relaxant activity and antihypertensive effect of benzo[d]imidazole derivatives. *Bioorg. Med. Chem.* **2010**, *18*, 3985-3991, https://doi.org/10.1016/j.bmc.2010.04.027.
91. Nguyen, G. Renin, (pro)renin and receptor: An update. *Clin Sci.* **2011**, *120*, 169–178, https://doi.org/10.1042/cs20100432.
92. Trott, O.; Olson, A.J. AutoDock Vina: Improving the speed and accuracy of docking with a new scoring function, efficient optimization and multithreading. *J. Comput. Chem.* **2010**, *31*, 455–561, https://doi.org/10.1002/jcc.21334.
93. Adegbola, A.E.; Fadahunsi, O.S.; Alausa, A.; Abijo, A.Z.; Balogun, T.A.; Aderibigbe, T.S.; Semire, B.; Adegbola, P.I. Computational prediction of nimbanal as potential antagonist of respiratory syndrome coronavirus. *Inform. Med. Unlocked.* **2021,** *24*, 100617, https://doi.org/10.1016/j.imu.2021.100617.
94. Adegbola, P.I.; Fadahunsi, O.S.; Adegbola, A.E.; Semire, B. *In silico* studies of Potency and safety assessment of selected trial drugs for the treatment of COVID-19. *In Silico Pharmacology* **2021**, *9*, 45, https://doi.org/10.1007/s40203-021-00105-x.
95. Oyebamiji, A.K.; Fadare, O.A.; Akintelu, S.A.; Semire, B. Biological Studies on Anthra[1,9-cd]pyrazol-6(2D)-one Analogues as Anti-vascular Endothelial Growth Factor Via In silico Mechanisms. *Chemistry Africa* **2021**, *4*, 955-963, https://doi-org.libproxy.viko.lt/10.1007/s42250-021-00276-2.
96. Adegbola, P.I.; Semire, B.; Fadahunsi, O.S.; Adegoke, A.E. Molecular docking and ADMET studies of Allium cepa, Azadirachta indica and Xylopia aethiopica isolates as potential antiviral drugs for Covid-19. *VirusDis.* **2021,** *32*, 85-97, https://doi.org/10.1007/s13337-021-00682-7.
97. Oyebamiji, A.K.; Akintelu, S.A.; Amao, O.P.; Kaka, M.O.; Morakinyo, A.E.; Amao, F.A.; Semire. B., Dataset on Theoretical Bio-Evaluation of 1,2,4-Thiadiazole-1,2,4-Triazole Analogues against Epidermal Growth Factor Receptor Kinase down Regulating Human Lung Cancer. *Data Brief* **2021**, *37*, 107234, https://doi.org/10.1016/j.dib.2021.107234.
98. B.; Rarey, M.; Lengauer, T. Evaluation of the FlexX incremental construction algorithm for protein ligand docking. *Proteins Struct. Funct. Bioinf.* **1999,** *37*, 228-241, https://doi.org/10.1002/(SICI)1097-0134(19991101)37:2%3C228::AID-PROT8%3E3.0.CO;2-8.
99. El-Azab, A.S.; Mary, Y.S.; Panicker, C.Y.; Abdel-Aziz, A.A.M.; El-Sherbeny, M.A.; Van Alsenoy, C. DFT and experimental (FT-IR and FT-Raman) investigation of vibrational spectroscopy and molecular docking studies of 2-(4-oxo-3-phenethyl-3,4-dihyroquinazolin-2-ylthio)-N-(3,4,5-trimethoxyphenyl) acetamide. *J. Mol. Struct.* **2016**, *1113*, 133-145, https://doi.org/10.1016/j.molstruc.2016.02.038.